Deliverable number: D1.1

Micromechanical model for fibre peel-off and pull-out

Frode Grytten, SINTEF

Bent F. Sørensen, DTU

Stergios Goutianos, DTU

Reidar K. Joki, FiReCo

Jens K. Jørgensen, SINTEF

The DACOMAT project has received funding from the European Union's Horizon 2020 research and innovation programme under GA No. 761072

Deliverable details

Document name: D1.1 Micromechanical model for fibre peel-off and pull-out

Responsible partner: SINTEF

Work package: WP1 - Concept Modelling

Task: 1.1: Micromechanical assessment of fibre bridging

Due date: 31.12.2019

Delivery date:31.12.2019

Revision history

Version	Date	Author / Reviewer	Notes
1.1	01.11.2019	Frode Grytten, SINTEF	
1.2	17.11.2019	Reidar Joki, FIRECO	
1.3	10.12.2019	Nicolas Krumenacker, SINTEF	English check
1.4	27.12.2019	Jens Kjær Jørgensen, SINTEF	Final review

Dissemination level	
x	PU = Public
	CO = Confidential, only for members of the consortium (including the EC)
	Classified, information as referred to in Commission Decision 2001/844/EC.
Deliverable type	
x	R: Document, report (excluding the periodic and final reports)
	DEM: Demonstrator, pilot, prototype, plan designs
	DEC: Websites, patents filing, press & media actions, videos, etc.
	OTHER: Software, technical diagram, etc.

The DACOMAT project has received funding from the European Union's Horizon 2020 research and innovation programme under GA No. 761072

Popular science summary

Fibre bridging in delaminating composites is a mechanically complex phenomenon. The tractions on the surface in a fracture zone with fibre bridging is the sum of forces from numerous individual fibres crossing between the fracture surfaces. The mathematical modelling of this is demanding and performing detailed simulations with for instance finite element analyses require enormous computational resources and large effort in pre and post processing. In DACOMAT a very efficient semi-analytical micromechanical model of fibre bridging describing the pull out, fracture and buckling of fibres has been developed. The model is in very good accordance with detailed finite element analyses but several magnitudes shorter calculation time. The model has shown to provide valuable input both for understanding how material properties affect fibre bridging and how cohesive laws for macroscale modelling can be defined.

Technical summary

A mathematical model describing crossover fibre bridging is established. The model is a semi-analytical micromechanical model based on the framework of Sørensen et al. [1] extended with von Kármán strains [2] and a Weibull distributed failure strain in the bridging fibres. The model includes the debonding of fibres from the matrix, buckling of bridging fibres in compression and ultimately rupture of fibres. The model's predictions are shown to be in excellent agreement with those resulting from detailed finite element models. Furthermore, the computational efficiency of the proposed model enables parametric studies that would be unfeasible using finite element models with similar accuracy. A small parametric study was conducted using the proposed model to demonstrate its feasibility. The most important finding from this preliminary parametric study is that increasing the fracture energy of the fibre/matrix interface may decrease the delamination resistance of laminates, because fibres rupture prematurely. This contradicts the current trends in sizing and matrix development, where still stronger interfaces are sought.

The DACOMAT project has received funding from the European Union's Horizon 2020 research and innovation programme under GA No. 761072

1.Introduction

The use of fibre reinforced composite laminates for structural applications has seen a remarkable increase over the past couple of decades. Significant weight and cost savings can be achieved by replacing conventional materials with composite laminates owing to their high specific properties and tailorability. Still, low fracture toughness through the thickness remains an important hurdle, as it can engender rapid delamination growth and lead to catastrophic failure.

Several techniques have been developed to increase through-thickness fracture toughness, including z-pinning, stitching and 3D weaving. Aside from such toughening methods, an intrinsic strengthening mechanism manifests itself in composite laminates under certain conditions known as *crossover fibre bridging*. This mechanism consists of fibres bridging a delamination in the wake of its crack front. By potentially acting as crack arrestors, fibre bridging can lead to increased delamination resistance.

Fibre bridging is typically attributed to the nesting of fibres from adjacent plies, which is most notable in unidirectional laminates. However, there is no consensus on the effect of ply orientation on the manifestation of fibre bridging [3]. In turn, Johnson et al. [4] reported that small ply angles of 1.5 and 3 degrees reduce the presence of fibre bridging. Lastly, Nicholls and Gallagher [5] reported that increasing the relative ply angle could activate a second bridging mechanism: the crack front does not necessarily propagate in parallel to the fibre axis and can thus deviate from the main crack plane into adjacent ply interfaces thereby ensuing in additional fibre bridging in the wake of new crack fronts.

Bradley and Cohen [6] identified yet another source of fibre bridging for tough resin matrices. They suggested that, in tougher resin matrices, the crack tip yield zone extends to several plies above and below the main delamination plane. Additional delamination cracks will appear throughout this extended zone which will eventually yield further fibre bridging as the delamination grows.

Micromechanical modelling of crossover fibre bridging allows for the study of its underlying mechanisms and potential approaches to harness this intrinsic mechanism such as to maximize fracture toughness and damage tolerance. Several micromechanical models have thus far been proposed to predict the macroscopic traction-separation laws for crossover fibre bridging.

Spearing and Evans [7] developed one such model for pure mode I delamination that includes shear deformations in a bridging "ligament" with a rectangular cross section [8]. Shear deformations are dominant for small crack opening displacements while the ligament is relatively short. In contrast, the shear deformations are negligible for large crack opening displacements when the ligament has been peeled from the fracture surface and become slenderer.

Kaute et al. [9] proposed a model whereby only the axial stiffness of the bridging fibre is considered. They modelled the bridging fibre as a straight beam with a large length to diameter ratio. In addition, they considered the reduction in tensile strain due to fibre slippage within the uncracked matrix by applying fracture-mechanic considerations. The model predicts that the normal tractions acting on the fracture surface from a single fibre will increase as function of opening displacement and eventually reach a plateau. A length-dependence of fibre strength was included through a Weibull distribution. In this way, the number of surviving fibres decreases for increasing opening displacements and the resulting traction on the fracture surface also decreases, as observed experimentally.

The DACOMAT project has received funding from the European Union's Horizon 2020 research and innovation programme under GA No. 761072

Sørensen et al. [1] proposed a micromechanical model for mixed-mode delamination based on classical Euler-Bernoulli beam theory. Their work can be viewed as an extension of the model by Spearing and Evans to mixed mode I/II delamination. The two models offer identical results for pure mode I crack opening if the shear term of Spearing and Evans is omitted. In such a case, both models predict the normal traction to be inversely proportional to the square root of the normal opening distance.

The models by Spearing and Evans [7] and Sørensen et al. [1] are limited to infinitesimally small deflections of the bridging fibre, i.e. when the local normal opening displacement is much smaller than the height of the bridging fibre. In contrast, the model proposed by Kaute et al. [9] is only applicable when the local normal opening displacement is several orders of magnitude greater than the height of the bridging fibre.

The scope of the present work is to establish a micromechanical model applicable to the full range of lateral deflections that bridging fibres are subjected to under mixed mode I/II delamination. The model is based on the framework of Sørensen et al. [1] and employs moderately large deflection beam theory and a Weibull distributed failure strain in the bridging fibres.

2.Mathematical model

A fracture process zone (FPZ) with bridging fibres and the corresponding equivalent tractions represented by macroscopic traction-separation laws are illustrated in Figure 1. A mathematical model for these traction-separation laws will be derived in this section.

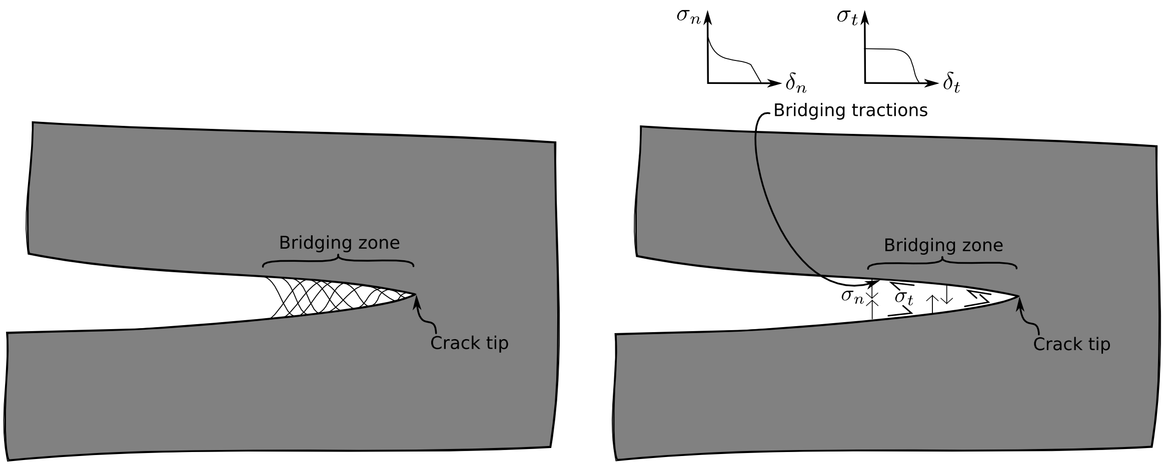

Figure 1. Fracture process zone with bridging fibres (left) and equivalent fracture process zone with bridging tractions (right).

Figure 2 shows a single bridging fibre located at an arbitrary position within the fracture process zone (FPZ). The fibre will be considered as a nonlinear beam. In the depicted case, the beam is fixed at the left end while the local opening displacements are imposed to the right end. The horizontal and vertical displacements associated with the right beam end are denoted δ_x and δ_y, respectively.

The DACOMAT project has received funding from the European Union's Horizon 2020 research and innovation programme under GA No. 761072

These displacements correspond to the local opening displacements that are prescribed in the model. Both ends of the beam are constrained from rotating. The prescribed end displacements result in varying displacements along the beam. The horizontal displacement as a function of position is denoted as u(x) and the corresponding vertical displacement is denoted as *w*(*x*).

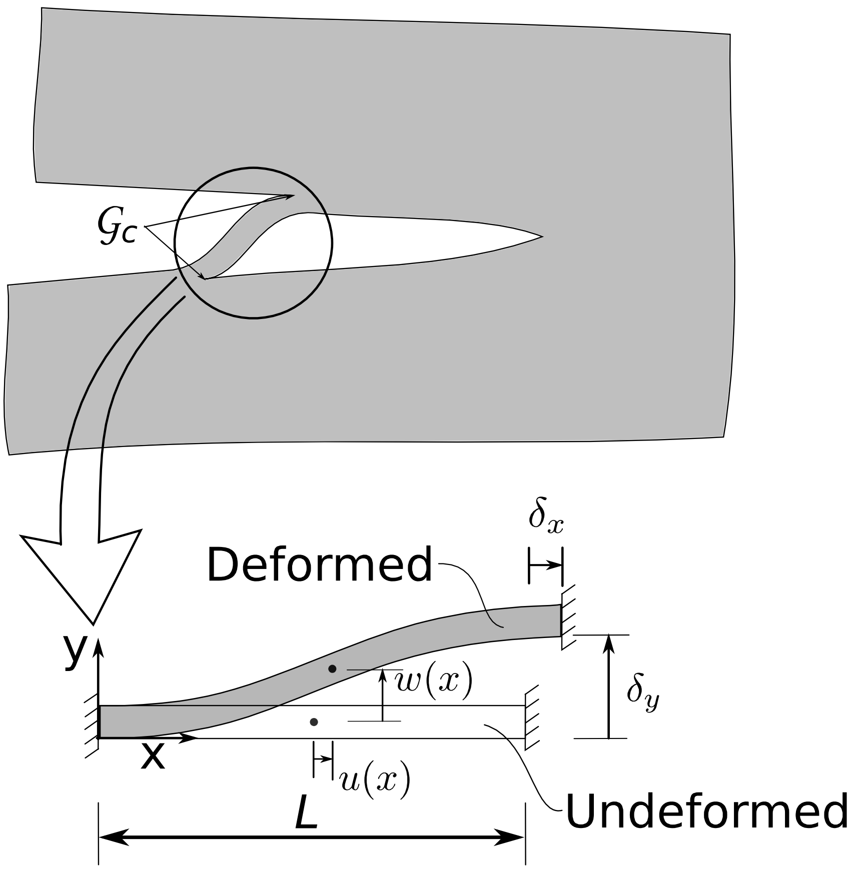

Figure 2. A single bridging fibre modelled as a beam.

The behaviour of the fibre material is assumed to be linear elastic, and the laws of elasticity remain unchanged from classical beam theory. The axial force *N* and bending moment *M* can be thus written:

$$N = EA\epsilon_n \tag{1}$$

$$M = EI\kappa \tag{2}$$

where E is the Young's modulus, A is the cross-sectional area, I is the second moment of area, ϵ_n is the strain at the neutral axis and κ is the curvature. Unlike classical beam theory, however, the expression for the axial strain at the neutral axis includes a second term to account for finite rotations (von Kármán strain [2]):

$$\epsilon_n = \frac{du}{dx} + \frac{1}{2}\left(\frac{dw}{dx}\right)^2 \tag{3}$$

The DACOMAT project has received funding from the European Union's Horizon 2020 research and innovation programme under GA No. 761072

Similarly, the definition of curvature also includes a nonlinear rotational term [10]:

$$\kappa = -\frac{\frac{d^2w}{dx^2}}{\left[1+\left(\frac{dw}{dx}\right)^2\right]^{3/2}} \tag{4}$$

Nevertheless, we will restrict our model to moderately large rotations where the square of the slope is small compared to unity. Curvature can thus be defined in the same way as in the small deflection theory:

$$\kappa = -\frac{d^2w}{dx^2} \tag{5}$$

The motivation for including the square of the slope in Equation (3) but not in (5) is that the fibre material is assumed to only experience small strains, i.e. $\frac{du}{dx} \ll 1$.

In turn, equilibrium in the vertical direction for a beam with non-zero axial force and no distributed vertical load is given by [10]:

$$-EI\frac{d^4w}{dx^4} + N\frac{d^2w}{dx^2} = 0 \tag{6}$$

where *N* is the still unknown axial force and *w* is the vertical displacement at a distance *x* from the left end of the beam. We assume the axial force as well as the cross-sectional properties to be constant along the beam. Eq. 6 is then divided by *EI* and the term $\lambda^2 = \frac{N}{EI}$ is introduced as follows:

$$\frac{d^4w}{dx^4} - \lambda^2\frac{d^2w}{dx^2} = 0 \tag{7}$$

Depending on the axial force, the general solution of this ordinary differential equation is:

$$\begin{aligned} w(x) &= C_0 + C_1x + C_2x^2 + C_3x^3 && \text{for } N = 0 \\ w(x) &= C_0 + C_1x + C_2cosh(\lambda x) + C_3sinh(\lambda x) && \text{for } N \neq 0 \end{aligned} \tag{8}$$

The constants C_0 to C_3 and the axial force must be determined from the boundary conditions. It should be noted that the constants will differ for the two cases ($N = 0$ and $N \neq 0$). The boundary conditions of the beam shown in Figure 2 are as follows:

$$\begin{gathered} u(0) = 0 \\ w(0) = 0 \\ w'(0) = 0 \\ u(L) = \delta_x \\ w(L) = \delta_y \\ w'(L) = 0 \end{gathered} \tag{9}$$

The DACOMAT project has received funding from the European Union's Horizon 2020 research and innovation programme under GA No. 761072

In the case of a constant axial force, Equations (8) and (9) form a system of four linear equations that must be solved simultaneously, and the following values can be determined for the four aforementioned constants:

$$\left.\begin{aligned} C_0 &= 0 \\ C_1 &= 0 \\ C_2 &= \frac{3\delta_y}{L^2} \\ C_3 &= \frac{-2\delta_y}{L^3} \end{aligned}\right\} \quad \text{for } N = 0$$
$$\left.\begin{aligned} C_0 &= \frac{\delta_y\big(1 - cosh(\lambda L)\big)}{2 - 2cosh(\lambda L) + \lambda L \sinh(\lambda L)} \\ C_1 &= \frac{\delta_y \lambda \sinh(\lambda L)}{2 - 2cosh(\lambda L) + \lambda L \sinh(\lambda L)} \\ C_2 &= \frac{\delta_y(cosh(\lambda L) - 1)}{2 - 2cosh(\lambda L) + \lambda L \sinh(\lambda L)} \\ C_3 &= \frac{-\delta_y sinh(\lambda L)}{2 - 2cosh(\lambda L) + \lambda L \sinh(\lambda L)} \end{aligned}\right\} \quad \text{for } N \neq 0 \qquad (10)$$

Since the axial force is assumed to be constant along the beam, it can be expressed in terms of the total beam elongation:

$$N = EA\frac{\Delta L}{L} \qquad (11)$$

The axial strain depends on both vertical and horizontal displacements *u* and *w* as written in Equation (3). The elongation of the beam can be determined from the integral of Equation 3 which equals the difference in horizontal movement at the ends plus the integral of the axial strain arising from vertical movement along the beam:

$$\Delta L = u(L) - u(0) + \int_0^L \frac{1}{2}\left(\frac{\mathrm{dw}}{\mathrm{dx}}\right)^2 \mathrm{dx} \qquad (12)$$

Inserting Equations (12) and (9) into (11) yields:

$$N = \frac{EA}{L}\left[\delta_x + \int_0^L \frac{1}{2}\left(\frac{dw}{dx}\right)^2 dx\right] \qquad (13)$$

Inserting Equations (8) into (13) results in a rather complicated transcendental equation for λ, from which no closed-form solution has been obtained. An iterative approach is instead used where N_{i+1} is found by inserting N_i into Equations (8) and (10) and using this in Equation (13). The vertical displacement *w*(*x*) calculated from linear theory (i.e. setting *N* = 0) can be used as a starting point for iteratively calculating the axial force.

Combining Equations (8) and (10) provides the solution for *N* = 0:

$$w_0(x) = \delta_y\left(\frac{3x^2}{L^2} - \frac{2x^3}{L^3}\right) \qquad (14)$$

The DACOMAT project has received funding from the European Union's Horizon 2020 research and innovation programme under GA No. 761072

Differentiating Equation (14), inserting into Equation (13) and performing the integral yields:

$$N_0 = \frac{EA}{L}\left(\delta_x + \frac{3\delta_y^2}{5L}\right) \tag{15}$$

This initial estimate is normally very good, and few iterations are needed to obtain acceptable accuracy.

Figure 3 illustrates two fibres crossing in the opposite directions. The equations derived above are valid for a fibre crossing from lower left to upper right. Similar expressions for a fibre crossing in the opposite direction are readily derived but will not be shown here.

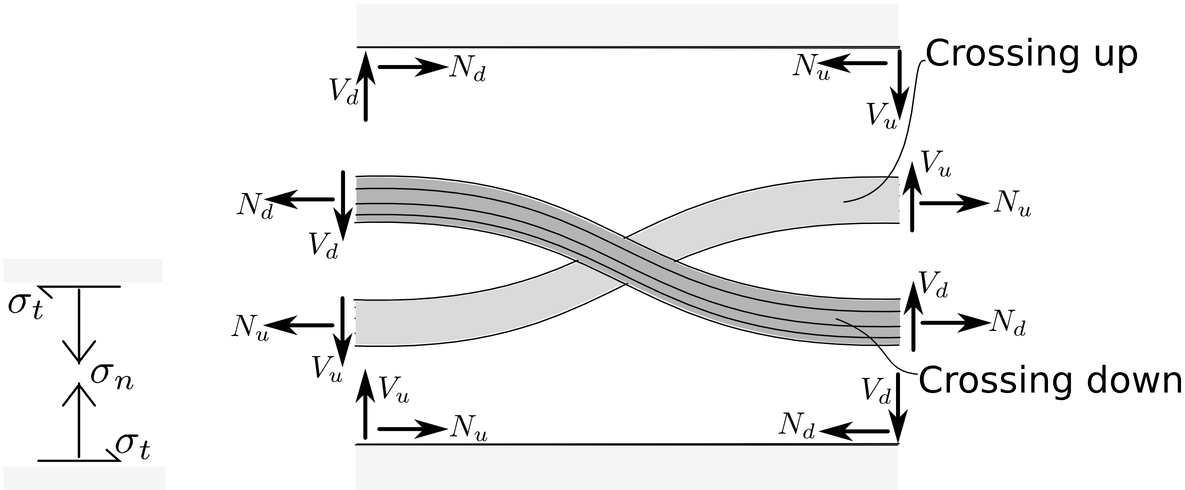

Figure 3. Two fibres crossing in opposite directions and sign convention of bridging tractions.

Figure 3 also illustrates the sign convention for bridging tractions and beam forces. Since beam ends are constrained from rotating, the horizontal force acting on the fracture surface from one beam is identical to the axial force *N*. Similarly, the vertical force is identical to the shear force *V* at the end of the beam. The shear force can be obtained by differentiating the bending moment, which is proportional to the curvature:

$$V(0) = M'(0) = -EIw'''(0) = \begin{cases} -6C_3EI & for \quad N = 0 \\ -\lambda^3 C_3 EI & for \quad N \neq 0 \end{cases} \tag{16}$$

Slender fibres are susceptible to buckling if they are subjected to compressive axial forces approaching the critical load, which for fixed ends can be written as follows:

$$N_{cr} = \frac{4\pi^2 EI}{L^2} \tag{17}$$

Therefore, no contribution to the bridging tractions are assumed for fibres meeting the buckling criterion $N < -N_{cr}$.

The DACOMAT project has received funding from the European Union's Horizon 2020 research and innovation programme under GA No. 761072

The forces in a bridging beam with given length *L* were derived above. The length of the beam must be determined for given opening displacements. If the FPZ of the debonding process between fibre and matrix is small, *L* can be determined by requiring that the potential energy release rate of the bridging mechanism equals the fracture energy of the interface G_c. The potential energy of an elastic body Π is defined as follows [11]:

$$\Pi = U - F \tag{18}$$

where *U* is the strain energy in the body and *F* is the work performed by external forces. When the displacement of the crack surfaces is fixed, $F = 0$ and $\Pi = U$. The rate of change in potential energy with the crack area *G* can thus be written as follows:

$$G = \frac{\partial \Pi}{\partial A} = \frac{\partial U}{\partial A} = \frac{\partial U}{b\, \partial L} \tag{19}$$

where A is the fracture area and b is the effective width of the fracture area. Since the material is assumed to be linearly elastic, the strain energy density can be calculated as:

$$\hat{u} = \frac{1}{2}\sigma\epsilon = \frac{\sigma^2}{2E} \tag{20}$$

The total strain energy can then be expressed as:

$$U = \int_V \hat{u} dV = \int_V \frac{N^2}{2EA^2} dV + \int_V \frac{M^2 y^2}{2E\mathrm{I}^2} dV = \frac{N^2 L}{2EA} + \frac{EI}{2}\int_0^L w''(x) dx \tag{21}$$

where y is the distance to the neutral axis. The first term is due to stretching and the second to bending. The bending moment *M* is expressed by $M(x) = -EIw''(x)$, where *w(x)* is the deflection of the nonlinear beam as described by Equation (8). Numerical differentiation is used in our implementation to determine $\frac{\partial U}{\partial L}$. The length *L* is determined from the equilibrium condition, $G = G_c$. In practice by solving the following equation using Newton's method:

$$G_c + \frac{1}{b}\frac{\partial U}{\partial L} = 0 \tag{22}$$

The contribution from both the normal and shear force to the fracture surface tractions depends on fibre orientation as illustrated in Figure 3. Let η_u and η_d be the number of fibres bridging a unit area of the fracture surface in the up and down diagonal direction, respectively. The tractions on the fracture surface can then be written as follows:

$$\begin{aligned} \sigma_t &= N_u\eta_u - N_d\eta_d \\ \sigma_n &= V_u\eta_u - V_d\eta_d \end{aligned} \tag{23}$$

where σ_t and σ_n are the tangential and normal tractions, respectively. The sign convention follows from Figure 3. The number of fibres currently bridging a unit area of the fracture surface is the product of the number of fibres bridging initially and the fraction of unbroken fibres:

$$\begin{aligned} \eta_u &= \eta_{u0}P_{su} \\ \eta_d &= \eta_{d0}P_{sd} \end{aligned} \tag{24}$$

The DACOMAT project has received funding from the European Union's Horizon 2020 research and innovation programme under GA No. 761072

The probability of survival of single fibres of length L under an applied homogeneous strain no greater than ϵ is described using the two-parameter Weibull distribution [12]:

$$P_s(\epsilon) = e^{\left[-\frac{L}{L_0}\left(\frac{\epsilon}{\epsilon_0}\right)^m\right]} \tag{25}$$

Where ϵ_0 and m are the respective Weibull scale and shape parameters for the failure strain and L_0 is the reference length at which these parameters are determined. The shape parameter m determines the coefficient of variation and the magnitude of the size effect, in addition to describing the flaw distribution. Previous experiments have shown that this approximation is reasonable for fibres subjected to uniform strain [12-14]. Assuming that fibres fail due to surface flaws when subjected to tension, the following surface integral can be used for fibres subjected to a heterogeneous strain field [15]:

$$P_s = e^{\left[-\frac{D}{2\pi D_0 L_0 \epsilon_0^m}\int_0^L \int_0^{2\pi} \langle\epsilon\rangle^m d\theta dx\right]} \tag{26}$$

Here ⟨⟩ indicate Macaulay brackets so that only tensile strains contribute to the likelihood of fibre failure.

Both the semi-analytical model and finite element analysis have shown that the largest combination of bending and axial strains occurs at the point of last contact between a partly pulled out fibre and the matrix. The largest contribution to the surface integral occurs at this cross-section. As the fibre continues to be pulled out, the previously strained cross-sections migrate away from the point of last contact and their contribution to the surface integral plummets. This is analogous to testing a chain by straining one link at the time, as illustrated in Figure 4. The integral in Equation (26) of such a test would be constant. The model does not capture size effects whereby the probability of failure due to a severe defect increases as more links in the metaphorical chain have become subjected to severe loading.

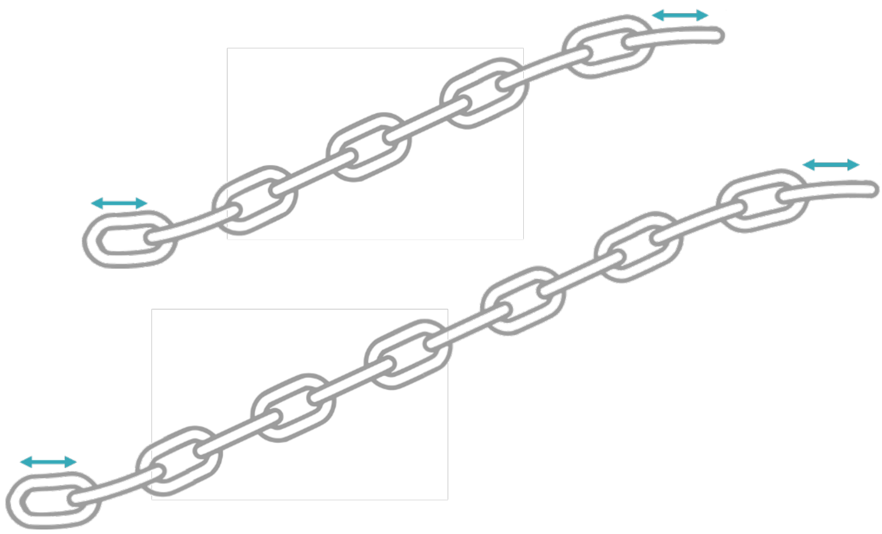

Figure 4. Straining mainly the end of the bridging ligament causes the surface integral at the current state to be less representative for the strain history the ligament has seen.

A more representative alternative to capture the fibres' strain history would be to integrate strains along the fibre's end circumference and then multiply by the fibre length as follows:

$$P_s = e^{\left[-\frac{DL}{2\pi D_0 L_0 \epsilon_0^m}\int_0^{2\pi}\langle\epsilon\rangle^m d\theta\right]} \tag{27}$$

3.Implementation of the model

Two different implementations of the model described in Section 2 have been made. The model was initially implemented as a set of MATLAB scripts. These require MATLAB, which is a proprietary software platform, but no additional MATLAB toolboxes. For this reason, a second implementation was made in Python, which is a free open-source platform. The latter has also been compiled to an executable stand-alone software that can run on Windows without any additional software requirements. All these implementations have been checked against each other to identify and correct any bugs. The MATLAB implementation has been further validated against finite element simulations as will be shown in Section 4.

A brief introduction to the stand-alone executable version is provided below. The distributable zip file contains two sample CSV files (model input and output examples) along with an executable file:

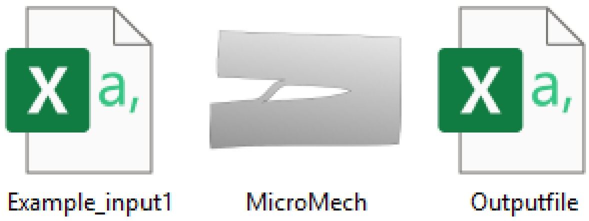

Upon double-clicking the MicroMech-icon, the user is prompted to select an input file:

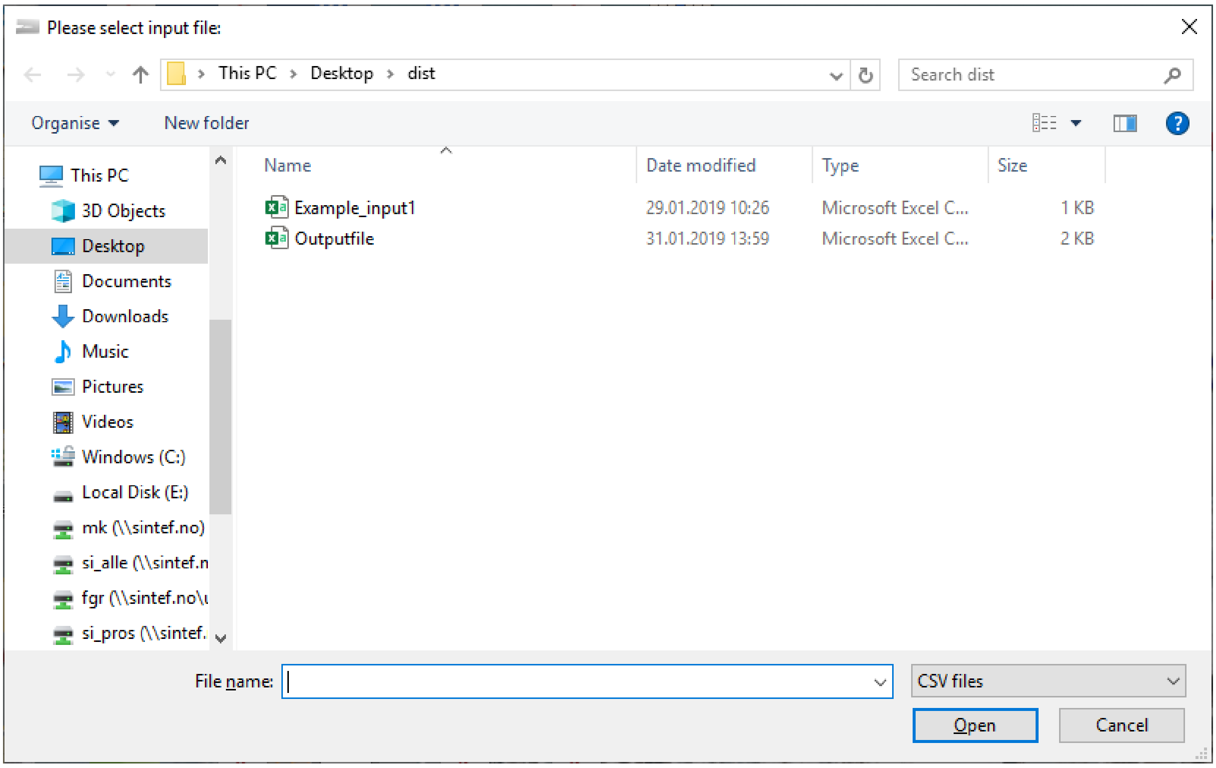

The DACOMAT project has received funding from the European Union's Horizon 2020 research and innovation programme under GA No. 761072

The program then prompts for the output file:

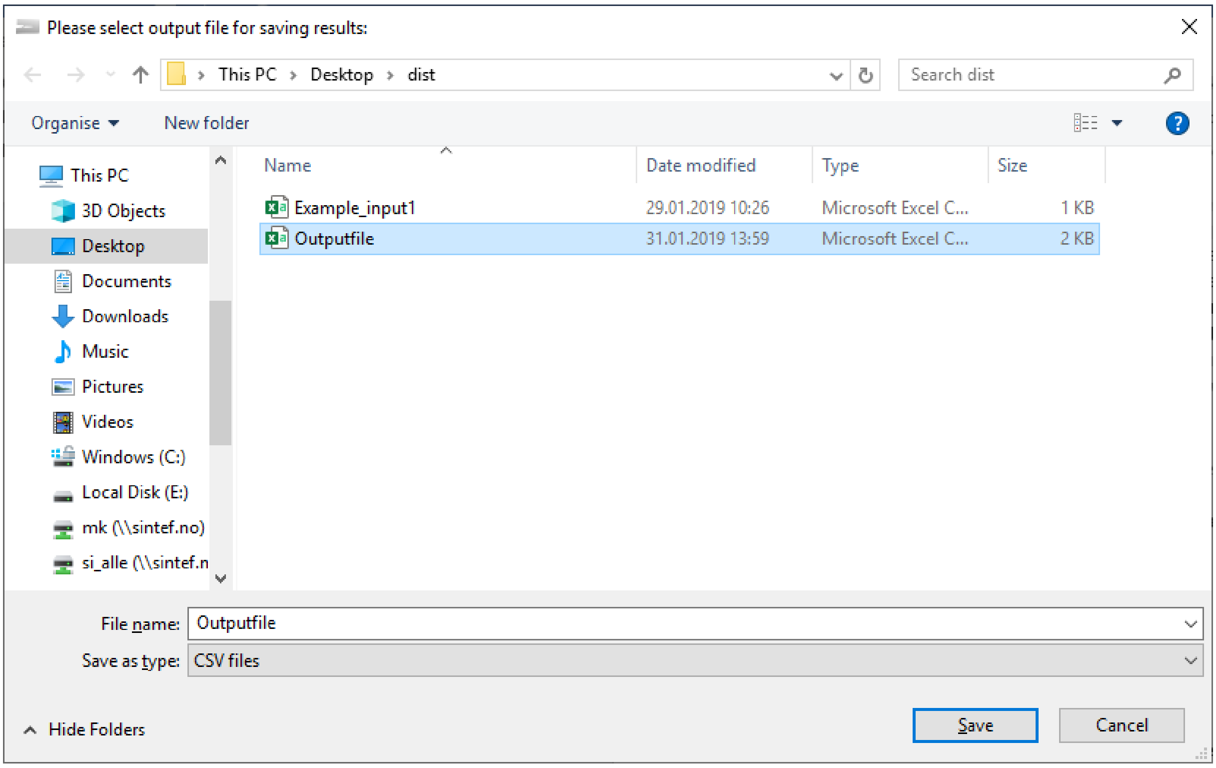

If an existing output file is selected, the program asks for confirmation to overwrite this file:

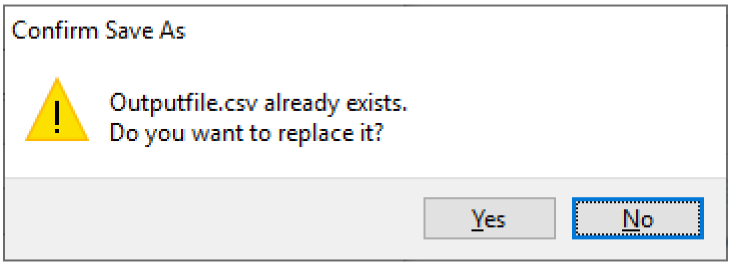

The various cases defined in the input file are then calculated. A message pops up once all the calculations have been completed and the results written to the output file:

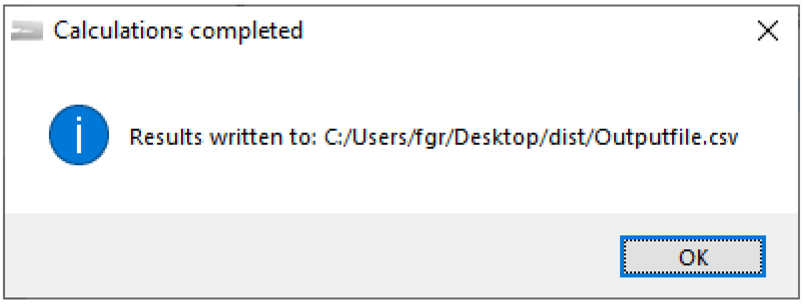

The DACOMAT project has received funding from the European Union's Horizon 2020 research and innovation programme under GA No. 761072

The results can then be imported to Excel or other appropriate programs for visualisation and further post processing. In addition, the software itself contains simple purpose-built plotting capabilities:

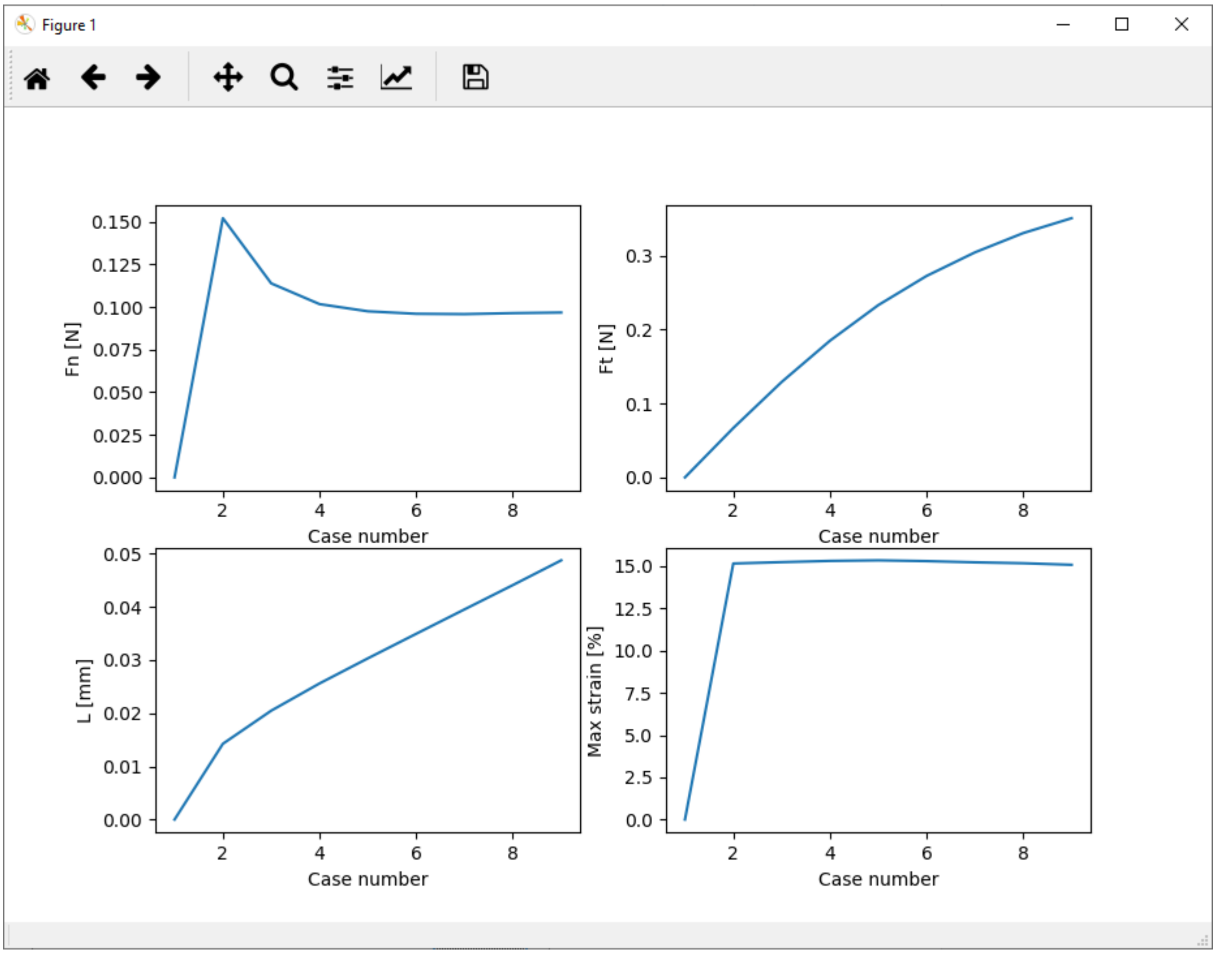

The figures can be saved in a variety of formats directly from the plotting tool:

Portable Network Graphics (*.png)

Encapsulated Postscript (*.eps)
Joint Photographic Experts Group (*.jpeg *.jpg)
PGF code for LaTeX (*.pgf)
Portable Document Format (*.pdf)
Portable Network Graphics (*.png)
Postscript (*.ps)
Raw RGBA bitmap (*.raw *.rgba)
Scalable Vector Graphics (*.svg *.svgz)
Tagged Image File Format (*.tif *.tiff)

The DACOMAT project has received funding from the European Union's Horizon 2020 research and innovation programme under GA No. 761072

The input variables appear as column headers in the first row of the input CSV file:

Gc	E	A	Iy	y_max	delta_n	delta_t
0.015708	72000	0.000314	4.91E-10	0.005	0	0
0.015708	72000	0.000314	4.91E-10	0.005	0.001	0
0.015708	72000	0.000314	4.91E-10	0.005	0.002	0
0.015708	72000	0.000314	4.91E-10	0.005	0.003	0
0.015708	72000	0.000314	4.91E-10	0.005	0.004	0
0.015708	72000	0.000314	4.91E-10	0.005	0.005	0
0.015708	72000	0.000314	4.91E-10	0.005	0.006	0
0.015708	72000	0.000314	4.91E-10	0.005	0.007	0
0.015708	72000	0.000314	4.91E-10	0.005	0.008	0

Example_input1

The output file contains all the input variables, and the calculated output variables are appended in the following columns:

	Gc	E	A	Iy	y_max	delta_n	delta_t	F_n	F_t	L	epsilon_max
0	0.015708	72000	0.000314	4.91E-10	0.005	0	0	0	0	0	0
1	0.015708	72000	0.000314	4.91E-10	0.005	0.001	0	0.152033	0.066729	0.014255	0.151529
2	0.015708	72000	0.000314	4.91E-10	0.005	0.002	0	0.114551	0.129511	0.020437	0.153002
3	0.015708	72000	0.000314	4.91E-10	0.005	0.003	0	0.102165	0.18545	0.025565	0.153592
4	0.015708	72000	0.000314	4.91E-10	0.005	0.004	0	0.097558	0.233175	0.030316	0.153538
5	0.015708	72000	0.000314	4.91E-10	0.005	0.005	0	0.096101	0.272654	0.034933	0.153086
6	0.015708	72000	0.000314	4.91E-10	0.005	0.006	0	0.095979	0.304691	0.039516	0.152437
7	0.015708	72000	0.000314	4.91E-10	0.005	0.007	0	0.096388	0.330444	0.044108	0.151725
8	0.015708	72000	0.000314	4.91E-10	0.005	0.008	0	0.096963	0.3511	0.048724	0.151026

Outputfile

In turn, each subsequent row corresponds to a particular case. In the above example, nine cases consist of identical variables except for the normal opening, which is increasing monotonically. In parametric studies such as the one presented in Section 5, G_c and E are the typical variables that would be varied.

The DACOMAT project has received funding from the European Union's Horizon 2020 research and innovation programme under GA No. 761072

4.Validation of the model

A comparison of the MATLAB implementation and nonlinear finite element simulation is presented in this section.

The first part of the mathematical model, namely Equations (1) to (16), predicts the forces resulting from translational movements of the right end of a beam with given length. Detailed finite element analyses were carried out in LS-DYNA in order to test both the applicability of the proposed model and its implementation. An arbitrary rectangular cross-section was chosen with a width of 5 mm and a height of 10 mm. The material was assumed to be linear elastic with a Young's modulus of 1GPa. Two beam lengths were selected:100 and 1000 mm. These were modelled using hexahedra elements with a characteristic length of 0.5 mm, see Figure 5. In this way, no assumptions of beam behaviour were made in the finite element analysis, and the models were capable of handling shear deformations and large rotations. Note that the chosen beam dimensions are not intended to be representative for bridging fibres but were chosen arbitrarily to test the model.

The boundary conditions were imposed by rigid bodies at both beam ends. The left rigid body (blue) was constrained from any movement (Figure 5). Vertical and horizontal translations were applied to the right rigid body (green).

Three different load cases were tested for both beams: 1) no horizontal displacement of the right end, 2) horizontal displacement with a magnitude corresponding to 90 % of the buckling load in 2) tension, and 3) horizontal displacement corresponding to 90 % of the buckling load in compression, then all followed by vertical displacement.

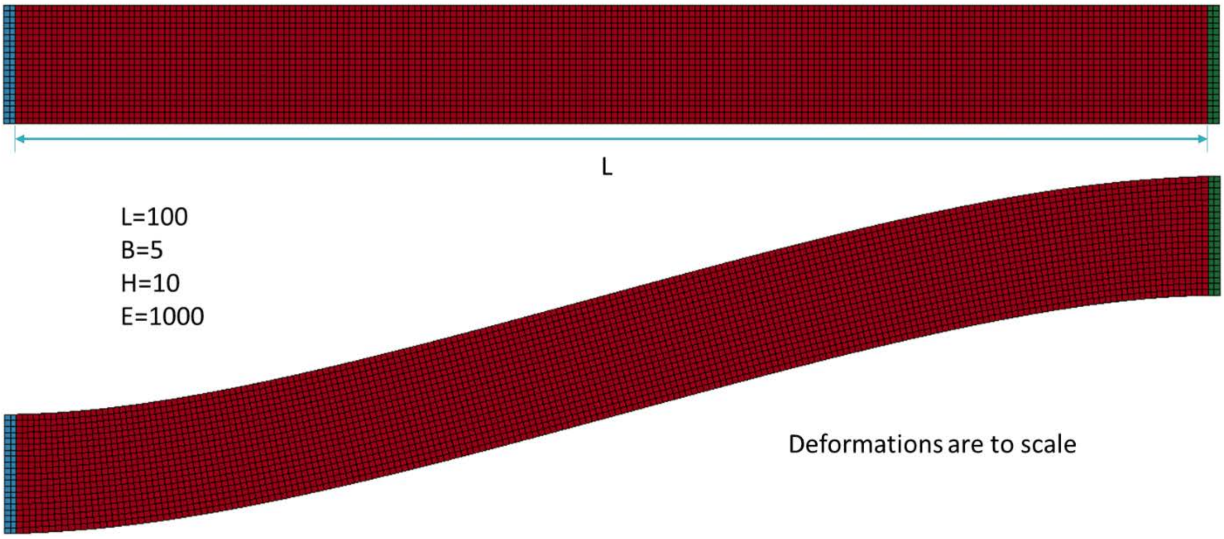

Figure 5. Finite element model of short beam capable of capturing shear deformations using hexahedra elements.

These initial simulations revealed that the response of a beam is highly nonlinear when lateral displacements approach or exceed the height of the beam. The normal and horizontal forces in the long slender beam subjected to only vertical displacements are shown in Figure 6 and Figure 7, respectively. At a displacement of 70 mm, linear beam theory predicts a vertical force that is approximately 3.5 % of the force predicted by the nonlinear model. Furthermore, linear beam theory predicts no horizontal force, however, the horizontal force is dominant in this problem, i.e. 13 times greater than the vertical force. This finding clearly demonstrates that nonlinear theory is required to predict the stresses and strains inside of a bridging fibre.

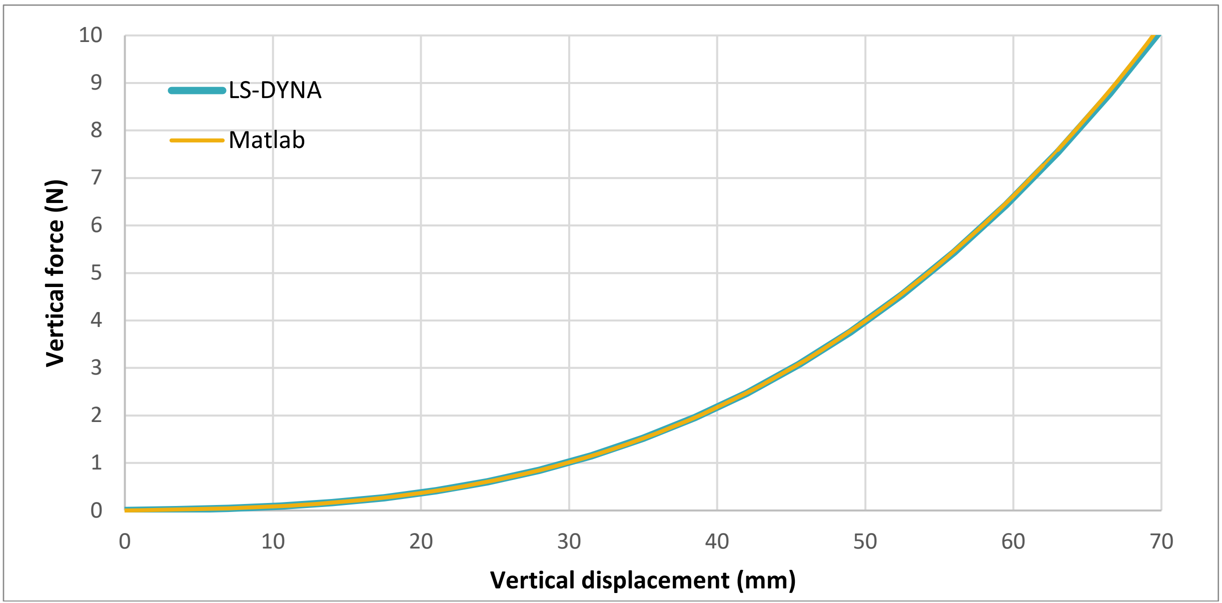

Figure 6. Vertical force as function of vertical displacement in the long slender beam.

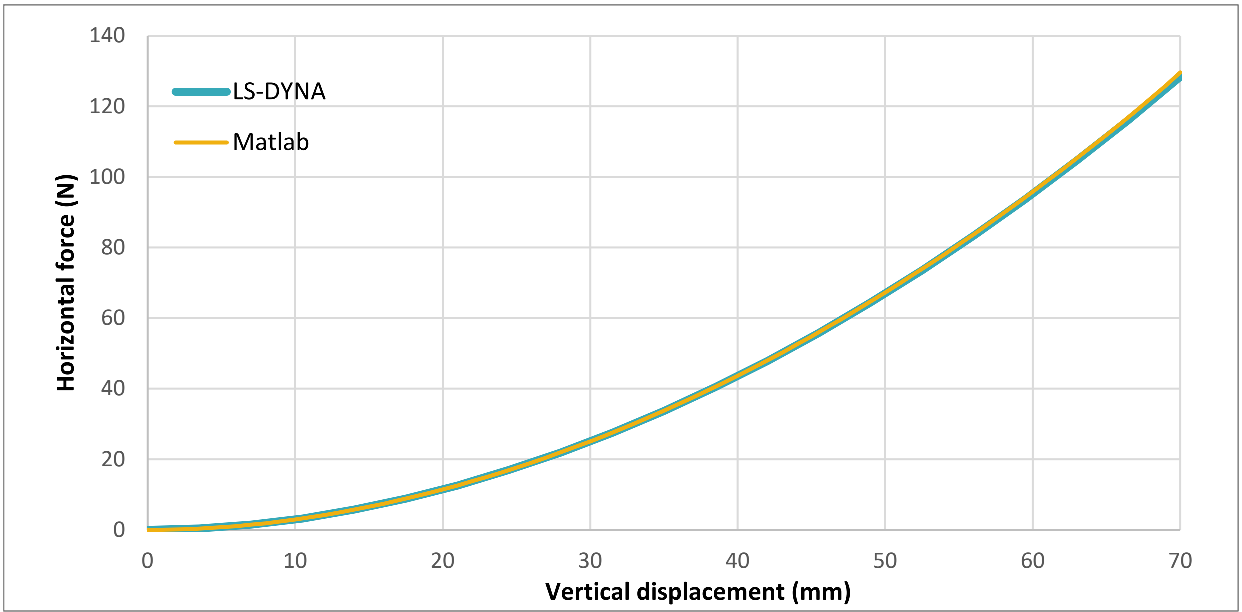

Figure 7. Horizontal force as function of vertical displacement in the long slender beam.

Figure 6 and Figure 7 demonstrate an excellent agreement between the finite element predictions and those of the proposed semi-analytical model for the case of a long and slender beam. However, some differences were observed for the short and bulky beam depicted in Figure 5. Figure 8, Figure 9 and Figure 10 show the vertical force as function of vertical displacement for a short beam with compressive preload, no preload and tensile preload, respectively. The difference between the finite element and semi-analytical model predictions is explained by the presence of shear deformations, which the proposed model does not include.

The geometric stiffness effect is well captured by the model, although error increases due to shear as the tensile force increases.

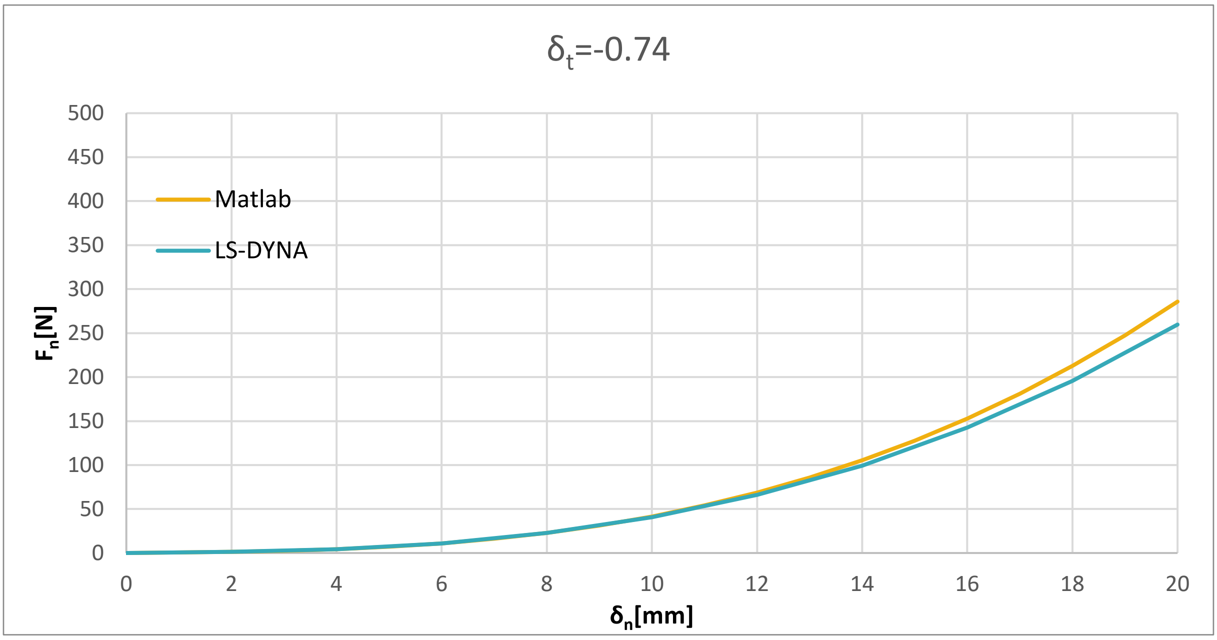

Figure 8. Vertical force in short beam preloaded in compression.

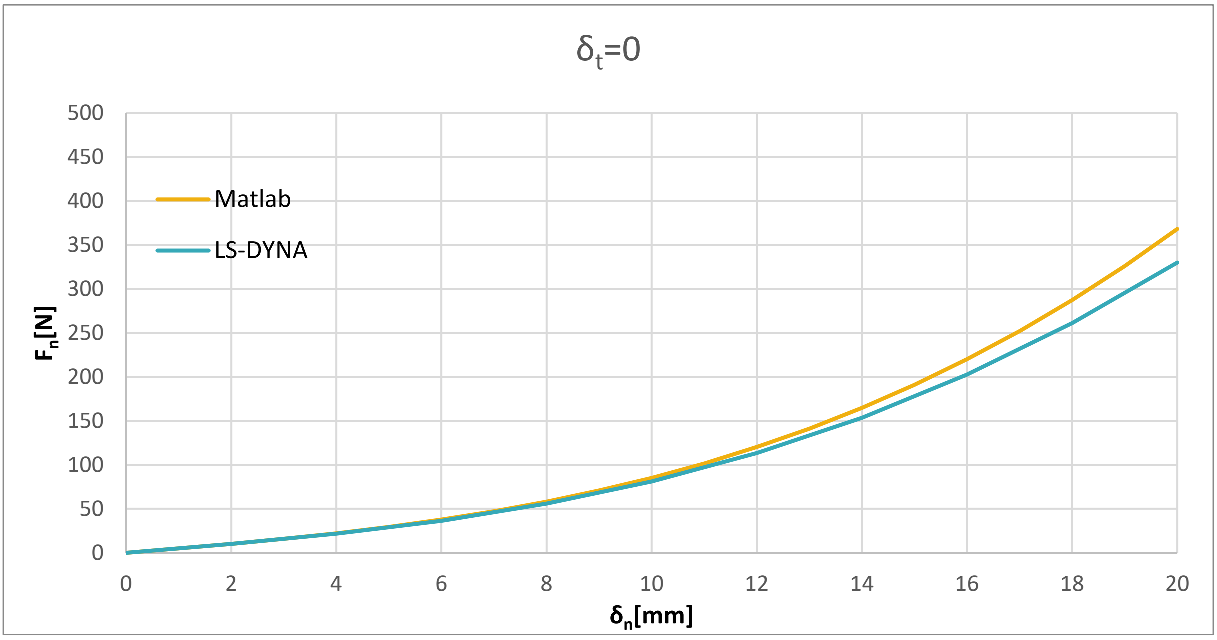

Figure 9. Vertical force in short beam without preload.

The DACOMAT project has received funding from the European Union's Horizon 2020 research and innovation programme under GA No. 761072

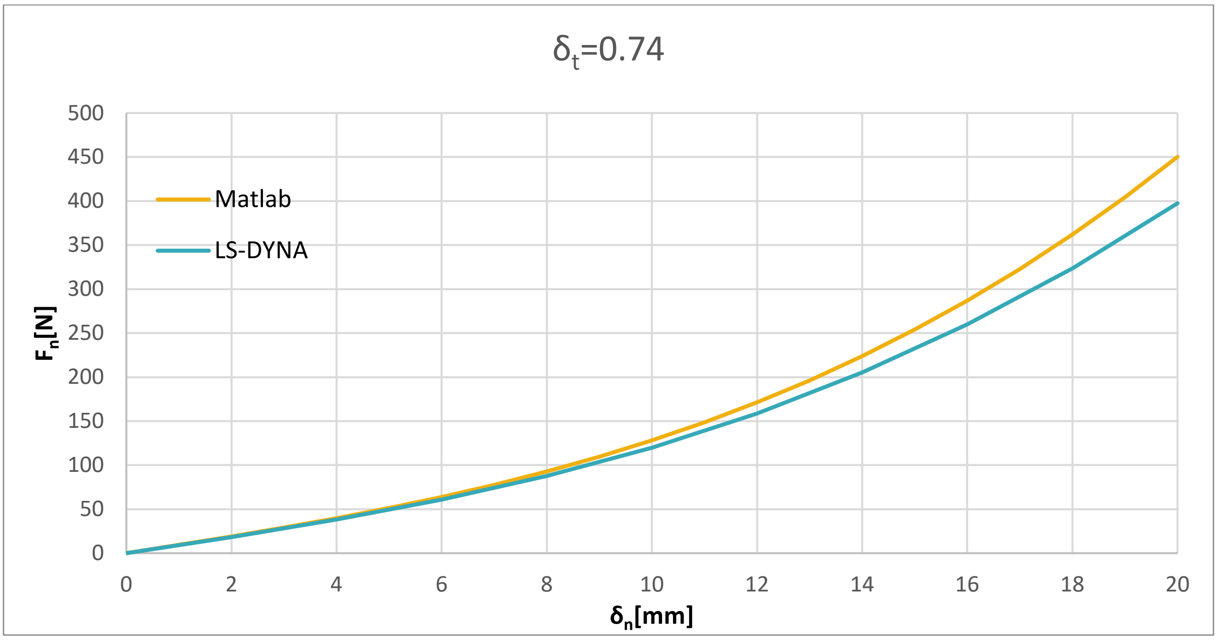

Figure 10. Vertical force in short beam preloaded in tension.

The DACOMAT project has received funding from the European Union's Horizon 2020 research and innovation programme under GA No. 761072

Buckling is governed by Equation (17) while the fibre peel-off is governed by Equations (18) to (22). These equations were validated using a separate finite element model depicted in Figure 11. The input parameters are summarized in Table 1 (reference case). A single elastic circular fibre was attached to two rigid fracture surfaces using cohesive elements. Both fibres crossing upwards and downwards were modelled and subjected to combinations of vertical and horizontal displacements. Selected results are summarized in Figure 12.

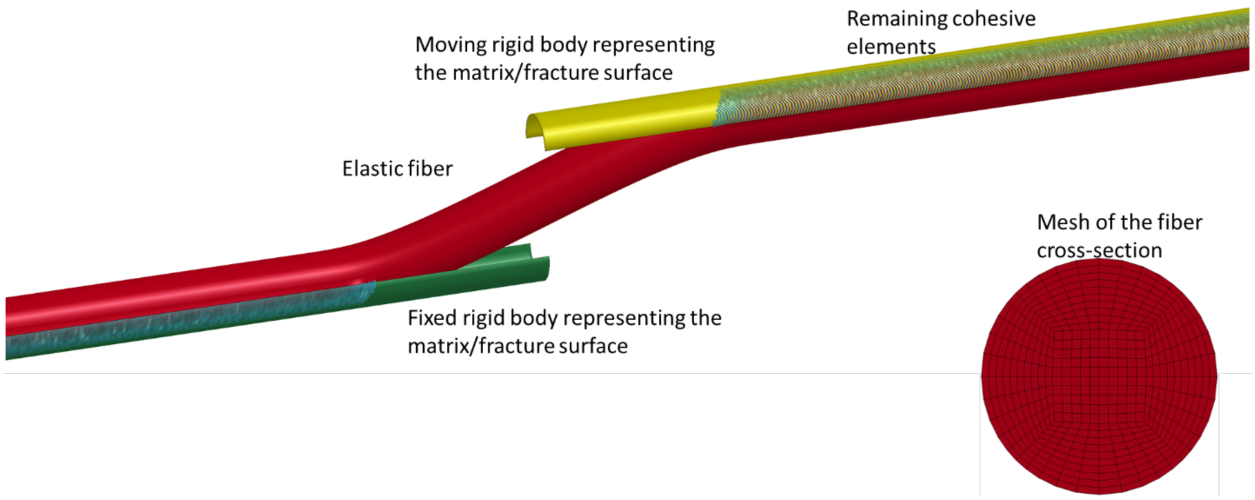

Figure 11. The finite element model used to validate the peel-off part of the proposed semi-analytical model.

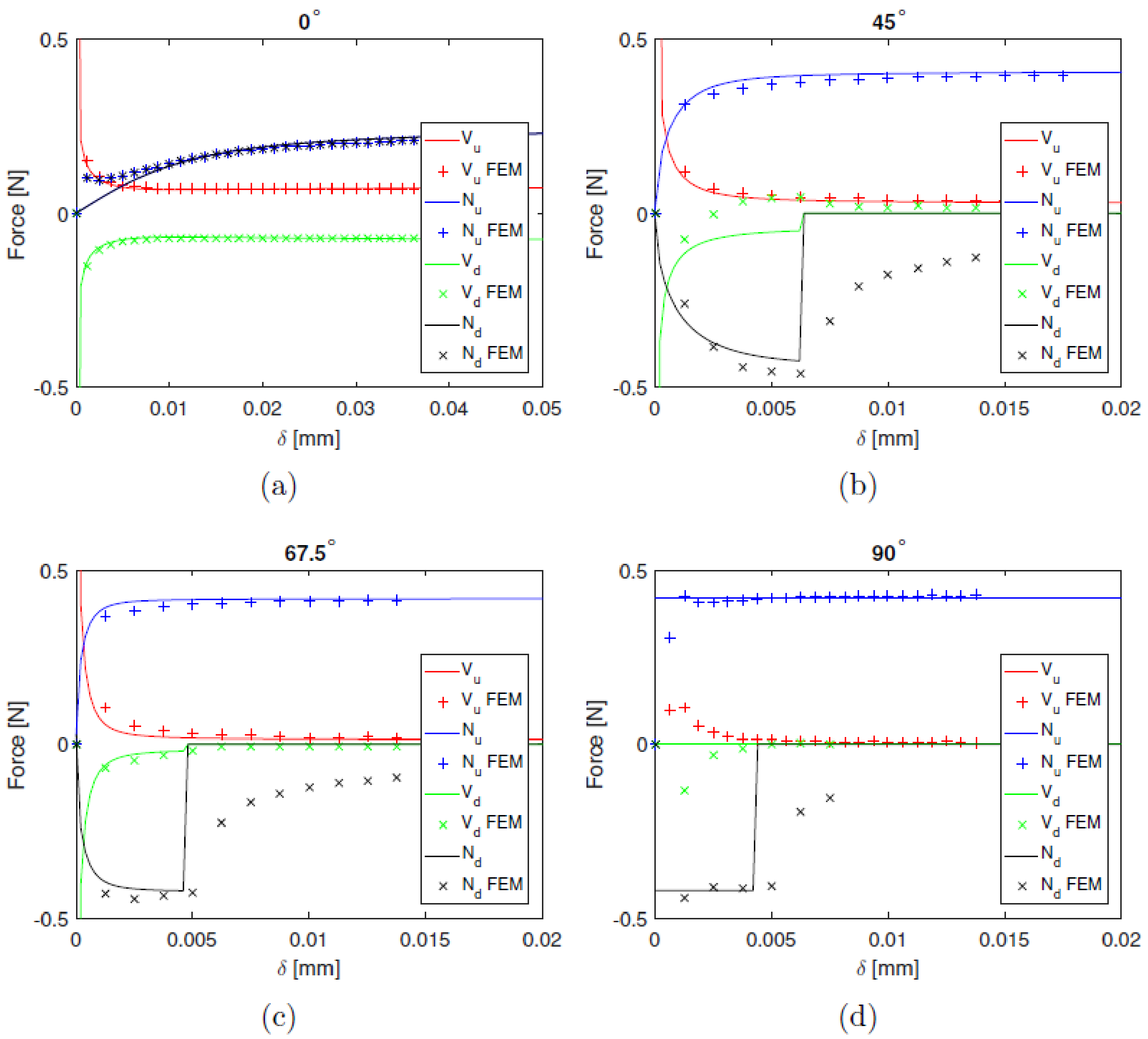

Figure 12. A comparison of tangential and normal force predicted by the finite element model and the nonlinear model: (a) Pure mode I; (b) ϕ = 45°; (c) ϕ = 67.5°; and (d) Pure mode II.

Figure 12 illustrates a very good agreement between the semi-analytical and FE models in the case of the predicted force level in tension and the onset bridging fibre buckling in compression. It should be noted that a limitation of the semi-analytical model is that the post-critical load carrying capability is neglected as forces are set to zero. See Figure 3 for a definition of the various forces.

A comparison between predictions of the normal force acting from a single fibre on the fracture surfaces made with the nonlinear model, a linear model and high-fidelity FEA is shown in Figure 13. Comparison of model predictions of the normal force acting on the fracture surfaces from a single fibre using the nonlinear model, linear model and high-fidelity finite element analysis (FEA). The overall agreement between FEA and our non-linear model is very good. They level off at the same force level, as opposed to the linear model which drops monotonically and too quickly. A linear model will underpredict the potential that bridging fibres have to transfer tractions. The semi-analytical model ran in a matter of seconds, while the FEA took some hours on the same PC. The FEA also ran into convergence issues at a normal opening displacement of approximately 0.05 mm.

The DACOMAT project has received funding from the European Union's Horizon 2020 research and innovation programme under GA No. 761072

The non-linear models seemingly reach a plateau for a single fibre. In reality, when there is a large number of fibres that progressively fail, the tractions would fall continuously due to fibre failures as shown in the next section.

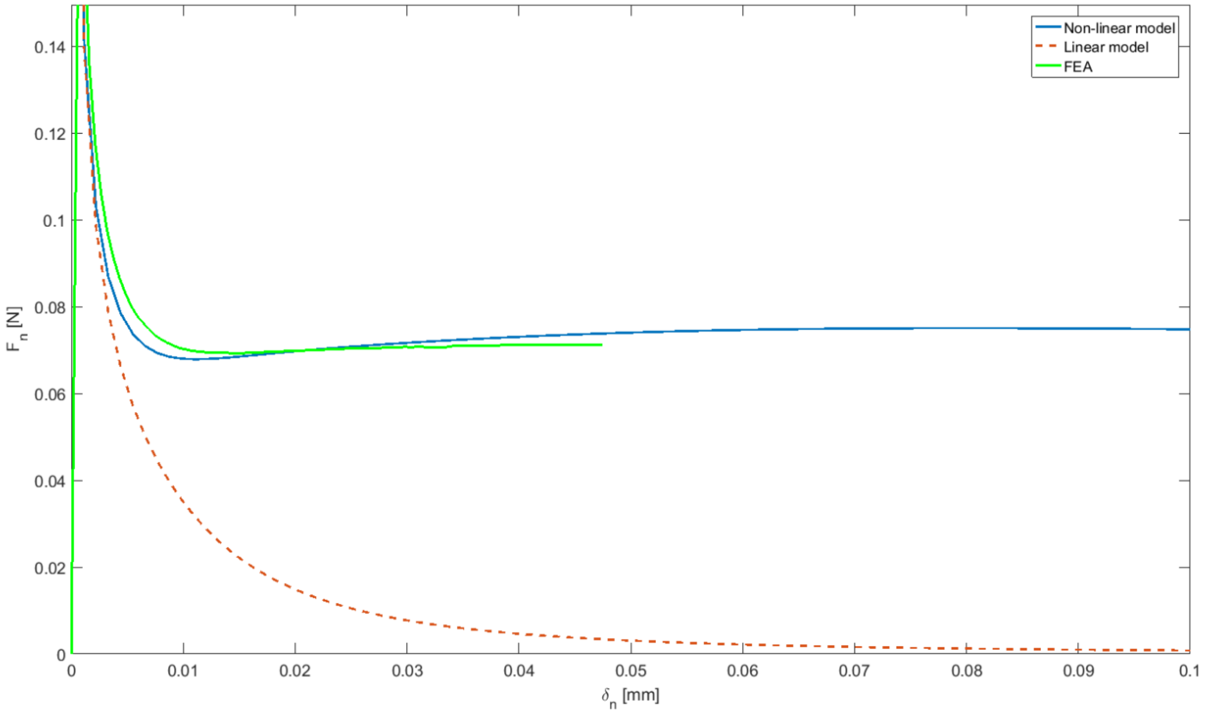

Figure 13. Comparison of model predictions of the normal force acting on the fracture surfaces from a single fibre using the nonlinear model, linear model and high-fidelity finite element analysis (FEA).

The DACOMAT project has received funding from the European Union's Horizon 2020 research and innovation programme under GA No. 761072

5. Parametric study

The proposed semi-analytical model has been used in a small parameter study to demonstrate its usefulness for such. The parameters varied were the fracture energy of the fibre – matrix interface and the fibre diameter. Note, that in the case where *D* was scaled, so was η to reflect a constant fibre volume fraction. The values of the input parameters used in this study are given in Table 1.

Table 1. Input parameters used to study effects of Gc and D.

	Reference	1.5G	2D
E_f	70 000 MPa	70 000 MPa	70 000 MPa
D	0.01 mm	0.01 mm	0.02 mm
G_c	1 Nmm/mm^2	1.5 Nmm/mm^2	1 Nmm/mm^2
m	6.4	6.4	6.4
ϵ_0	3.62%	3.62%	3.62%
L_0	70 mm	70 mm	70 mm
η_0	1 mm^{-2}	1 mm^{-2}	0.25 mm^{-2}

For simplicity, only pure mode-I and -II delaminations were investigated in this small study. The predicted bridging laws (traction-separation curves from bridging) for mode-I and mode-II are shown in Figure 14 and Figure 15, respectively. The energy dissipated through the bridging mechanism can be found by integrating the traction-separation curve. The resulting curves are shown in Figure 16 and Figure 17. As can be seen, increasing G_c leads to a more rapid decrease in tractions and therefore the dissipated energy is reduced. This effect is stronger in mode-I than in mode-II.

The DACOMAT project has received funding from the European Union's Horizon 2020 research and innovation programme under GA No. 761072

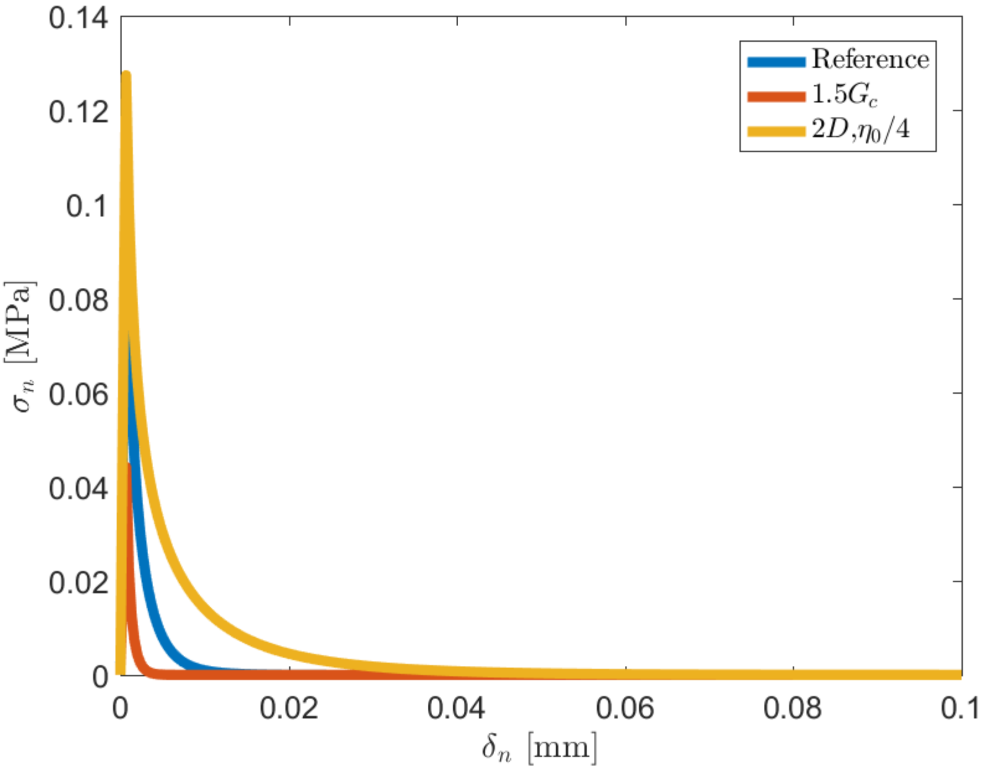

Figure 14. Normal traction as function of normal opening displacement in pure mode-I delamination.

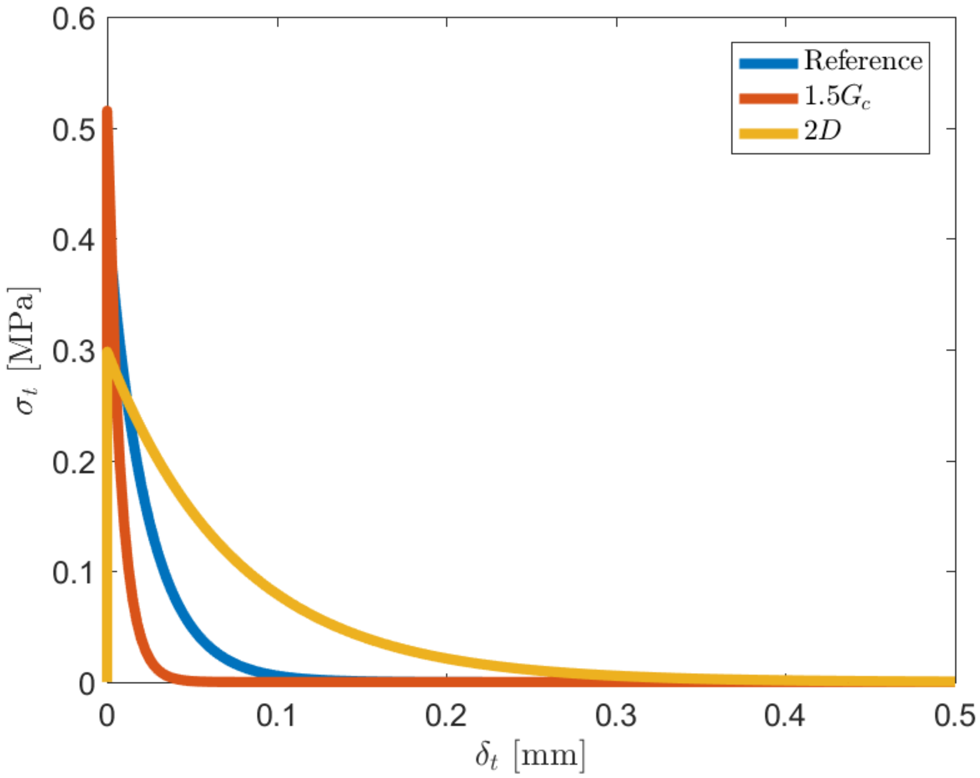

Figure 15. Tangential traction as function of tangential opening displacement in pure mode-II delamination.

The DACOMAT project has received funding from the European Union's Horizon 2020 research and innovation programme under GA No. 761072

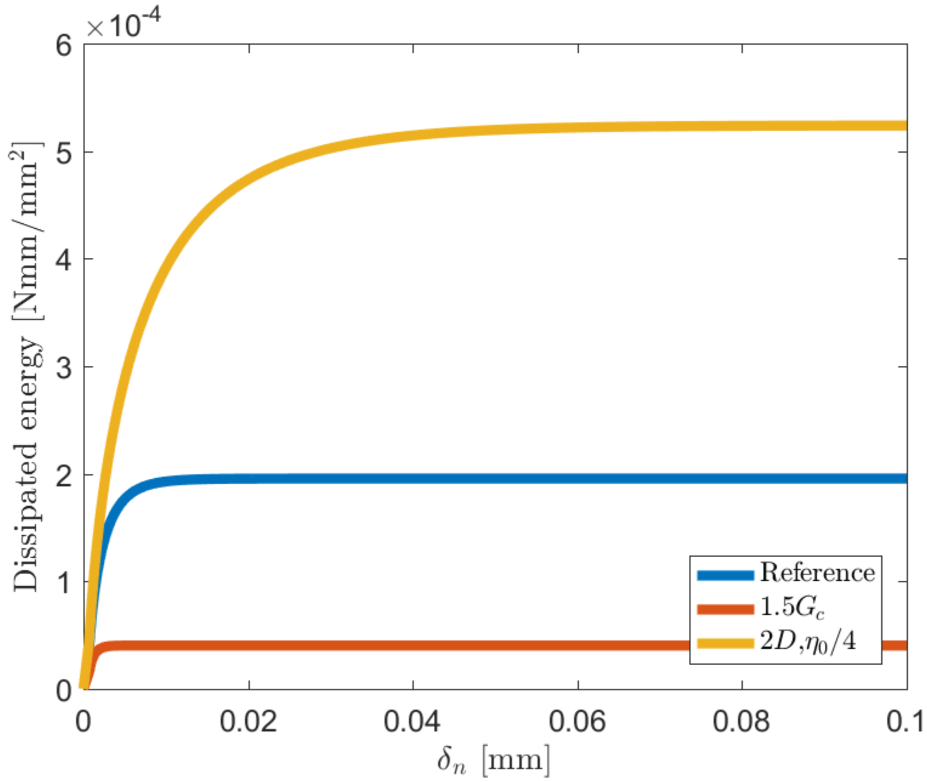

Figure 16. Energy dissipated through bridging in pure mode-I delamination.

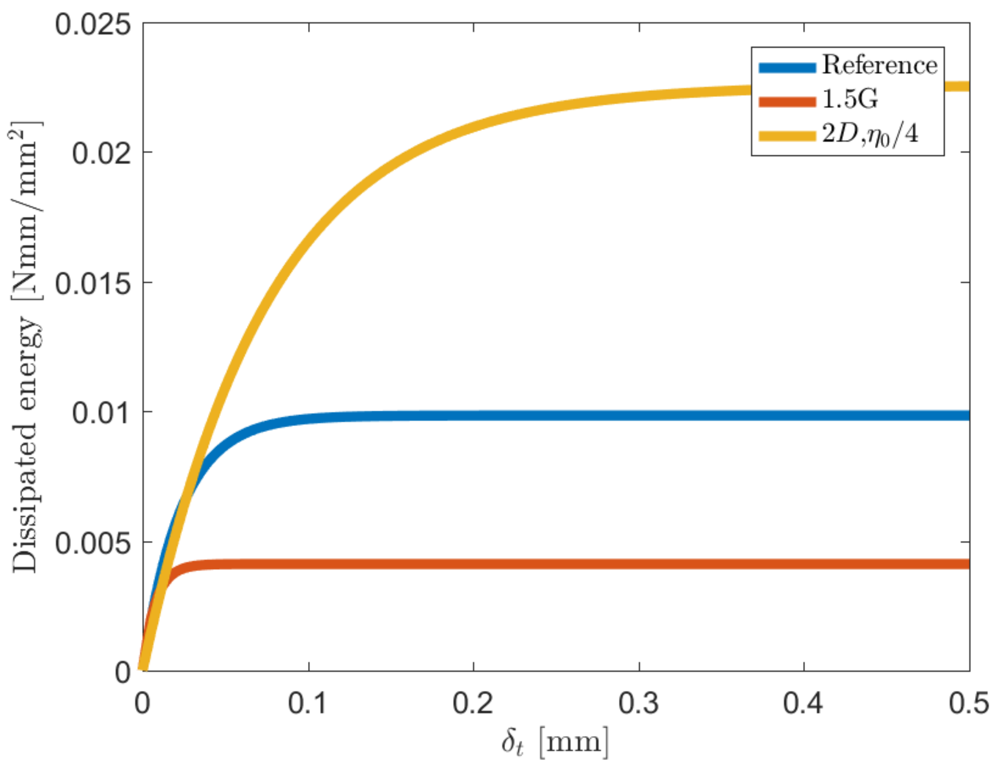

Figure 17. Energy dissipated through bridging in pure mode-II delamination.

6.Conclusions

A novel micromechanical model for crossover fibre bridging has been developed and validated against a high-fidelity finite element model. The model includes the debonding of fibres from the matrix, buckling of bridging fibres in compression and ultimately rupture of fibres.

The proposed model is based on moderately large deflection beam theory and therefore valid for the full range of deflections that bridging fibres are subjected to. The importance of considering large deflections was demonstrated for crossover fibre bridging by comparing predictions from linear and nonlinear models.

The proposed model is semi-analytical in nature and therefore much more computationally efficient than a comparable FE model. This advantage allows for parametric studies to be conducted.

A small parametric study was conducted to demonstrate the feasibility of using the proposed model in such studies. Fibre bridging was found to more greatly contribute to energy dissipation in mode-II than in mode-I. The most important model prediction is that increasing the fiber – matrix interface strength may actually decrease the delamination resistance of the laminate as fibres rupture prematurely.

Further parametric studies should be carried out to map the effects of a larger set of variables at mixed modes.

References

1. Sørensen, B.F., et al., *Micromechanical model of cross-over fibre bridging - Prediction of mixed mode bridging laws.* Mechanics of Materials, 2008. **40**(4-5): p. 220-234.
2. Von Kármán, T., *Festigkeitsprobleme im maschinenbau*. 1910, Leipzig: [publisher not identified].
3. Khan, R., *Fiber bridging in composite laminates: A literature review.* Composite Structures, 2019. **229**: p. 111418.
4. Johnson, W.S. and P.D. Mangalgiri, *INVESTIGATION OF FIBER BRIDGING IN DOUBLE CANTILEVER BEAM SPECIMENS.* Journal of Composites Technology and Research, 1987. **9**(1): p. 10-13.
5. Nicholls, D.J. and J.P. Gallagher, *Determination of GIC in Angle Ply Composites Using a Cantilever Beam Test Method.* Journal of Reinforced Plastics and Composites, 1983. **2**(1): p. 2-17.
6. Bradley, W. and R. Cohen, *Matrix Deformation and Fracture in Graphite-Reinforced Epoxies*, in *STP876-EB Delamination and Debonding of Materials*, W. Johnson, Editor. 1985, ASTM International: West Conshohocken, PA. p. 389-410.
7. Spearing, S.M. and A.G. Evans, *The role of fiber bridging in the delamination resistance of fiber-reinforced composites.* Acta Metallurgica Et Materialia, 1992. **40**(9): p. 2191-2199.
8. Timoshenko, S. and J.N. Goodier, *Theory of elasticity*. 1969: McGraw-Hill.
9. Kaute, D.A.W., H.R. Shercliff, and M.F. Ashby, *Delamination, fibre bridging and toughness of ceramic matrix composites.* Acta Metallurgica et Materialia, 1993. **41**(7): p. 1959-1970.
10. Fertis, D.G., *Nonlinear Mechanics*. 2 edition ed. 1999: CRC Press.
11. Anderson, T.L., *Fracture Mechanics, Fundamentals and Applications*. 2nd Edition ed. 1994: CRC Press.
12. Hill, R. and E.U. Okoroafor, *Weibull statistics of fibre bundle failure using mechanical and acoustic emission testing: the influence of interfibre friction.* Composites, 1995. **26**(10): p. 699-705.
13. Cowking, A., et al., *Testing E-glass fibre bundles using acoustic emission.* Journal of Materials Science, 1991. **26**(5): p. 1301-1310.
14. Evans, K.E., B.D. Caddock, and K.L. Ainsworth, *Statistical changes during the corrosion of glass fibre bundles.* Journal of Materials Science, 1988. **23**(8): p. 2926-2930.
15. Sørensen, B.F. and S. Goutianos, *Micromechanical model for prediction of the fatigue limit for unidirectional fibre composites.* Mechanics of Materials, 2019. **131**: p. 169-187.

The DACOMAT project has received funding from the European Union's Horizon 2020 research and innovation programme under GA No. 761072